Analytical and Bioanalytical Chemistry
https://doi.org/10.1007/s00216-020-02641-5

RESEARCH PAPER

Surface plasmon resonance sensing of Ebola virus: a biological threat

Pushpendra K. Sharma[1] · Jyoti S. Kumar[1] · Virendra V. Singh[1] · Utpal Biswas[1] · Shyam S. Sarkar[1] · Syed I. Alam[1] · Paban K. Dash[1] · Mannan Boopathi[1] · Kumaran Ganesan[1] · Rajeev Jain[2,3]

Received: 13 February 2020 / Revised: 19 March 2020 / Accepted: 3 April 2020

Abstract

Here, different monoclonal antibodies (mAb1, mAb2 and mAb3) of Ebola virus were screened in a real-time and label-free manner using surface plasmon resonance (SPR) to select an appropriate antibody for biosensor applications against a biological warfare agent. For this purpose, a gold SPR chip was modified with 4-mercaptobenzoic acid (4-MBA), and modification was confirmed by FTIR-ATR and EIS. The 4-MBA-modified gold SPR chip was used for immobilization of the recombinant nucleoprotein of Ebola (EBOV-rNP), and the interactions of mAb1, mAb2 and mAb3 were then investigated to determine the best mAb based on the affinity constant (K_D), expressed as equilibrium dissociation constant. K_D values of 809 nM, 350 pM and 52 pM were found for the interaction of mAb1, mAb2 and mAb3 of Ebola with the immobilized EBOV-rNP, respectively, thus reflecting the high affinity of mAb3. This was confirmed by ELISA results. The thermodynamic parameters (ΔG, ΔH and ΔS) for the interaction between mAb3 and EBOV-rNP were also determined, which revealed that the interaction was spontaneous, endothermic and driven by entropy. The SPR limit of detection of EBOV-rNP with mAb3 was 0.5 pg ml^{-1}, showing mAb3 to be the best high-affinity antibody in our study. This study has opened up new possibilities for SPR screening of different monoclonal antibodies of BWA through the convergence of materials science and optical techniques.

Keywords Nucleoprotein · Ebola virus · Bioweapon · Surface plasmon resonance · Biosensing

Introduction

In recent years, there have been alarming situations involving exotic viral infections which pose a high risk to health systems, and the malicious use of these viruses could be catastrophic. The ability of viruses to cause deadly epidemics in human societies opens an avenue for possible use as biological warfare agents (BWA) [1]. The world recently witnessed the largest and deadliest outbreak of Ebola virus disease (EBOV), which spread quickly in several countries of West Africa, resulting in high mortality rates, with more than 11,000 deaths. The evolving risk of the use of EBOV as a BWA attack, representing a threat to national security [2, 3], caused the World Health Organization (WHO) to declare it an international public health emergency [4]. This led to heightened awareness and visibility of the outbreak, sensitized public health officials and stimulated the international community to fight against this viral infection capable of causing mass destruction. Hence, EBOV is considered a potential candidate for use as a bioweapon [5].

The EBOV is a member of the *Filoviridae* family of viruses, and contains a non-segmented, negative-sense single-stranded RNA genome of approximately 19 kb that encodes seven proteins [6–8]. Viral proteins such as VP35, VP30 and the RNA-dependent RNA polymerase (L), along with the nucleoprotein (NP), are essential for viral replication and transcription. Viral protein VP40 is critical for virion assembly and budding, while viral protein VP24 is involved in the formation of nucleocapsid [9]. Among these proteins, NP is an ideal target antigen for the development of a rapid and sensitive detection methodology, owing to its abundance and strong antigenicity [10]. Monoclonal antibodies (mAbs) have

Electronic supplementary material The online version of this article (https://doi.org/10.1007/s00216-020-02641-5) contains supplementary material, which is available to authorized users.

✉ Mannan Boopathi
boopathi@drde.drdo.in

[1] Defence Research & Development Establishment, DRDO, Jhansi Road, Gwalior 474002, India

[2] School of Studies in Chemistry, Jiwaji University, Gwalior 474011, India

[3] Pondicherry University, Puducherry 605014, India

Published online: 19 April 2020

proven to be the basis for the development of simple, inexpensive, rapid and sensitive detection methods, and for enhanced immunoassay sensitivity and specificity [11–15].

Though the global proliferation of biological weapon technologies is restricted by the Biological Weapons Convention (BWC), EBOV may be used by terrorist organizations or enemy nations to gain power, as no effective vaccine or treatment is available for this EBOV infection. Hence, there is an urgent need to develop methods for the early detection of EBOV within the current scenario of BWA preparedness in order to control and contain its spread and to ensure timely treatment of infected persons. Various methodologies are available for the detection of EBOV in biological samples, such as reverse transcription polymerase chain reaction [16] and enzyme-linked immunosorbent assay (ELISA) [17]. However, these techniques have their own drawbacks, such as time-consuming, labor-intensive procedures, expensive equipment, low sensitivity and susceptibility to contamination during the amplification process, making them unsuitable for real-time detection of EBOV in real samples [18, 21]. Thus there is a need for a rapid, robust, label-free EBOV biosensor capable of real-time detection in order to address the current shortcomings.

Monoclonal antibodies are known for their extremely high specificity towards their antigen in sensing applications, and have shown promise in a number of potential applications in the detection of viral infections [22]. Surface plasmon resonance (SPR) is a versatile technique [21, 22] for the screening of antibodies by virtue of their affinity towards the antigen, and offers many advantages over conventional techniques. SPR has been a continuing focus of the scientific community in the development of plasmonic sensors for the real-time and label-free detection of bimolecular interactions [23–26].

Here, an SPR methodology was developed for screening of different monoclonal antibodies (mAb1, mAb2 and mAb3) of EBOV in a real-time and label-free manner to select an appropriate antibody for the development of a biosensor utilizing immobilized recombinant Ebola nucleoprotein (EBOV-rNP) on a 4-mercaptobenzoic acid (4-MBA)-modified SPR gold chip (EBOV-rNP/4-MBA/Au). Characterization of the 4-MBA/Au SPR chip was performed using SPR, electrochemical impedance spectroscopy (EIS) and attenuated total reflectance Fourier transform infrared spectroscopy (FTIR-ATR) in order to confirm the modification. Based on the affinity constant, the best antibody was selected and subsequently used for detection of EBOV-rNP in phosphate-buffered saline (PBS) medium. The other physical parameters including pH and temperature were optimized in order to elucidate the effective interaction of EBOV-rNP and mAb3. Kinetic and thermodynamic parameters were also calculated to determine the feasibility of interaction.

Materials and methods

Chemicals and reagents

4-MBA, *N*-(3-dimethylaminopropyl)-*N*′-ethylcarbodiimide hydrochloride (EDC), *N*-hydroxysuccinimide (NHS), phosphate-buffered saline (PBS), sodium acetate, ethanolamine and hydrochloric acid were purchased from Sigma-Aldrich. Glacial acetic acid, glycine, sodium hydroxide and methanol were also supplied by Sigma-Aldrich. Chemicals used in this work were of analytical grade, and purification was performed prior to use wherever necessary.

Instruments

An Autolab Spincoater (Eco Chemie B.V., Utrecht, Netherlands) was used for the uniform deposition of 4-MBA on the bare gold SPR chip. The interactions between antigen and antibodies were investigated using an Autolab ESPRIT SPR instrument (Eco Chemie B.V.) and a diode laser of 670-nm wavelength in conjunction with a scanning mirror. Different buffer solutions of different pH ranging from 4.0 to 9.0 were prepared and measured with a pH meter. Milli-Q water was used throughout the experiments. The temperature of the cuvette, syringe and microtiter plate was maintained as required using a Julabo HE-4 water bath. A 4800 Plus MALDI-TOF/TOR analyzer was utilized to characterize the EBOV-rNP.

Production of recombinant nucleoprotein of Ebola virus (EBOV-rNP)

The EBOV-rNP was custom-synthesized and cloned into cloning vector pUC18 and then subcloned in expression vector pET-22b. This was then subjected to transformation into *E. coli* BL21 (DE3) cells according to a standard protocol. A restriction digestion method was adopted to confirm the positive clones followed by nucleotide sequencing. To express NP, recombinant clones were induced with different concentrations of IPTG (0.5 to 2 mM in increments of 0.5 mM) in Luria broth (LB) media and checked periodically after every hour up to a period of 5 h. The cell suspension was sonicated followed by centrifugation at 18,600×*g* for 30 min at 4 °C in order to identify the localization of recombinant protein. After centrifugation, the remaining pellet and supernatant were collected separately followed by their analysis on 10% sodium dodecyl sulfate–polyacrylamide gel electrophoresis (SDS-PAGE) [27, 28]. Purification and characterization of EBOV-rNP were performed using SDS-PAGE, Western blot analysis and matrix-assisted laser desorption/ionization–time-of-flight mass spectrometry (MALDI-TOF/MS) analysis (for details]of EBOV-rNP characterization refer to Electronic

Supplementary Material (ESM) sections S1, S2 and S3, respectively).

Generation and purification of mAbs against EBOV-rNP

Four-week-old BALB/c mice were primed intraperitoneally with 50 μg EBOV-rNP protein mixed with Freund's complete adjuvant (Sigma, USA). Booster doses were given at 7-day intervals for 21 days. Splenocytes were isolated and allowed to fuse with SP2/0 myeloma cells in a ratio of 5:1 using 50% (*w*/*v*) polyethylene glycol according to a standard protocol [29, 30]. High-affinity clones were used to generate ascites in BALB/c mice, and mAb was purified by protein G chromatography according to the manufacturer's instructions (Amersham Pharmacia, Sweden). The concentration of monoclonal antibody was determined by BCA protein assay. For animal experiments, the study protocol for all experiments (no. Viro-14/57/PKD) was approved by the Institutional Animal Ethics Committee (IAEC) established through the Committee for the Purpose of Control and Supervision of Experiments on Animals (CPCSEA), Ministry of Environment and Forestry, Government of India (regd. no. 37/GO/Rbi/S/99/CPCSEA).

EBOV-rNP-based indirect ELISA

A total of 300 ng/well of the purified EBOV-rNP was coated in a 96-well microtiter plate using 0.1 M carbonate bicarbonate buffer (pH 9.6) and kept overnight at 4 °C. The coated wells were washed with PBS, and 3% bovine serum albumin (BSA) was used for blocking and kept overnight at 4 °C. The wells were washed again with 0.05% PBST and then incubated for 1 h at 37 °C with 100 μl of serially twofold-diluted (0.5 μg/ml) monoclonal antibodies against EBOV-rNP. Wells were again washed using the above procedure and incubated with anti-mice horseradish peroxidase (HRP) conjugate (1:5000 in PBS + 3% BSA). The wells were washed with 100 μl of TMB and incubated for 15 min at 37 °C. An aliquot of 100 μl of 1 N H_2SO_4 was used to terminate the enzyme reaction, and the absorbance was recorded at 450 nm.

Preparation and characterization of 4-MBA-modified gold chip

4-MBA modification of the SPR gold chip was carried out using a spin coater. An aliquot of 0.01 M 4-MBA methanolic solution (75 μl) was dispensed on a bare gold chip at 100 rpm for 3 min. The spin coater speed was then increased to 2500 rpm for 10 min in order to achieve a homogenous coating of 4-MBA on the SPR gold chip. The 4-MBA-modified SPR gold chip was characterized with SPR, EIS and FTIR-ATR. This 4-MBA-modified SPR gold chip was utilized for further modification and sensing studies.

Immobilization of EBOV-rNP on 4-MBA-modified gold SPR sensor chip for the screening of different mAbs of Ebola

Prior to the immobilization of EBOV-rNP on the 4-MBA-modified gold chip, PBS buffer (pH 7.5, 50 μl) was passed to obtain a stable baseline every 120 s (until obtaining the same change in SPR angle in both channels). The carboxylic group of 4-MBA is inactive for reaction with the amine group of proteins; hence, to make it active, the 4-MBA-modified gold chip was chemically treated with 400 mM EDC and 100 mM NHS by the injection of 50 μl of a 1:1 mixture. Then, 50 μl of EBOV-rNP (1:10 dilution in 10 mM PBS) was injected in channel 2 for 1800 s to obtain firm immobilization of EBOV-rNP on the activated 4-MBA-modified gold chip surface. After EBOV-rNP immobilization, the remaining active sites were blocked with 50 μl of 1 M ethanolamine to avoid cross-reactivity. Next, regeneration of the immobilized sensor surface was achieved with 10 mM HCl. The modified gold surface was activated with EDC/NHS and then blocked with ethanolamine (channel 1) for use in negative control experiments. The interaction of the immobilized EBOV-rNP sensor chip with different concentrations of mAb1, mAb2 and mAb3 of Ebola virus was then examined in order to select the best of the three antibodies based on their affinity constant, which was deduced from kinetic analysis.

Immobilization of mAb3 on 4-MBA-modified gold SPR sensor chip

Initially, before the immobilization of mAb3 on the 4-MBA-modified gold chip, stabilization of the experimental baseline in dual channels was carried out with 50 μl of PBS buffer (pH 7.5) every120 s until the same change in the SPR angle was observed in both channels. The 4-MBA-modified gold chip was chemically activated by the injection of 50 μl of a 1:1 mixture of 400 mM EDC and 100 mM NHS. Subsequently, 50 μl of mAb3 (1:10 dilution in 10 mM PBS) was injected in channel 2 for 1800 s to obtain effective immobilization of mAb3 on the activated 4-MBA-modified gold chip surface. Blocking of the remaining active sites and regeneration of the modified gold surface were carried out in a similar manner as that described in materials and methods section. For SPR sensing of EBOV-rNP, an aliquot of the analyte solution (50 μl) was injected and mixed at 16.7 μl/s, and this protocol was adopted with different dilutions of EBOV-rNP of 1:12,800, 1:6400, 1:3200, 1:1600, 1:800 and 1:400 to obtain a calibration plot and to determine the kinetic and thermodynamic parameters.

Optimization of experimental conditions

Temperature optimization

Analysis of temperature variation was carried out to investigate the effect of temperature on the change in SPR response [31]. To determine the optimum temperature for binding of mAb3 and EBOV-rNP, experiments were conducted by passing EBOV-rNP with a dilution of 1:12,800 (EBOV-rNP) on immobilized mAb3 with temperature varying from 13 to 34 °C in 3 °C increments (for details refer to ESM section S4).

pH optimization

It is well known that pH is a critical parameter that plays a key role in the study of biomolecular interactions and can also influence the sensitivity of SPR measurement. The effect of pH on the change in SPR response was investigated using different buffers by varying the pH from 4.0 to 9.0 (for details refer to ESM section S5).

Results and discussion

Expression, purification and characterization of EBOV-rNP

This EBOV-rNP gene was custom-synthesized and expressed into the pET-22b expression vector. The optimal expression of the 81 KDa EBOV-rNP was observed with induction of 0.5 mM and 1 mM IPTG for 5 h in the induced clone (Fig. 1a). The purification of the EBOV-rNP was performed under denaturing conditions. The protein was then eluted with the pH gradient and was found to be approximately 95% pure by gel analysis. The yield of pure recombinant envelope protein was estimated to be 10 mg L^{-1} of shake-flask culture.

Purified EBOV-rNP was characterized using Western blot and MALDI-TOF-TOF analysis. Western blot analysis of rNP with commercial rabbit anti-Ebola NP monoclonal antibody showed reactivity at the 81 KDa protein band, representing immunological activity of EBOV-rNP (Fig. 1b).

The EBOV-rNP was identified by MS/MS analysis of tryptic peptides using MALDI-TOF-TOF. The protein was identified as nucleoprotein from Ebola virus [gi|355,344,223] with a MASCOT score of 173 and sequence coverage of 8% using MS/MS data. A total of six peptides were matched to the protein through a MASCOT database search with significant ion score using the mass list of MS/MS fragment ions (Table 1).

Generation of monoclonal antibody against EBOV-rNP

A total of six hybridoma cell lines that produced mAbs against EBOV-rNP recombinant protein antigen were established. These mAbs specific to NP were obtained by immunization with the purified recombinant EBOV-rNP protein. The high-affinity mAbs were selected on the basis of strong positive reactions with EBOV-rNP recombinant protein by indirect ELISA.

Electrochemical impedance spectroscopy and FTIR-ATR characterization of modified gold SPR chip

To confirm the modification of 4-MBA on the SPR gold chip, characterization was carried out using electrochemical impedance spectroscopy (EIS) and FTIR-ATR. EIS is a versatile technique for determining interfacial parameters such as

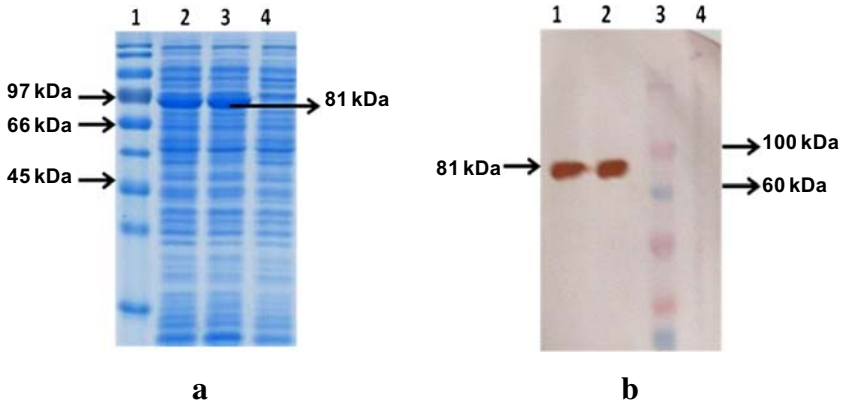

Fig. 1 (**a**) SDS-PAGE analysis of expressed EBOV-rNP. Lane 1: protein marker. Lanes 2 and 3: induced recombinant clone (0.5 and 1 mM IPTG). Lane 4: uninduced recombinant clone. (**b**) Western blot of recombinant protein (EBOV-rNP) showing reaction at ~81 kDa. Lanes 1 and 2: reaction of induced recombinant clone with anti-Ebola rabbit NP antibody (Abcam). Lane 3: pre-stained protein marker. Lane 4: pre-immunized control rabbit serum

Table 1 Identification of recombinant nucleoprotein of EBOV by MS/MS analysis of tryptic peptides using MALDI-TOF-TOF

Peptides	m/Z (Da)	Error (Da)	Position	Ion score
ILTAGLSVQQGIVR.Q	1454.9502	0.0813	24–37	46
YLEGHGFR.F	978.5448	0.0656	98–105	35
HGEYAPFAR.L	1047.5717	0.0711	290–298	22
EAATEAEKQLQQYAESR.E	1952.0197	0.0842	345–361	21
QLQQYAESR.E	1122.6362	0.0824	353–361	29
TPTVAPPAPVYR.D	1268.7915	0.0917	601–612	22

The protein was identified as nucleoprotein from Ebola virus [gi|355,344,223] with a MASCOT score of 173 (RMS error 64) and sequence coverage of 8% on MS/MS data

solution resistance (Rs), charge transfer resistance (Ret) and capacitance (C). Interfacial parameters are the most influential and direct parameters which reflect the in situ changes occurring at the modified chip/electrolyte interface. Hence, a modified Randles circuit (Rs (Q [Ret W]) fit and a simulation model were adopted to determine the Rs, Ret and C values for the bare gold and modified gold chips. As shown in Fig. 2, the semicircle diameter at higher frequency corresponds to the charge transfer-limited process (Ret), which was described by a parallel combination of C and Ret [32]. As shown in Fig. 2a, the bare SPR gold chip showed a small electron transfer resistance, with Ret of 0.776 kΩ, revealing enhanced electron transfer. After modification of the gold chip with 4-MBA (Fig. 2b), the diameter of the semicircle was increased, with Ret of 1.078 kΩ, indicating increased electron transfer resistance after modification with 4-MBA [33]. Rs and C values for the bare and modified SPR gold chips were also calculated and are presented in Table 2.

The 4-MBA-modified SPR chip was also characterized for its functional groups using FTIR-ATR. The FTIR-ATR spectrum of the bare gold chip is shown in Fig. 3a. Figure 3b shows the FTIR-ATR spectra for the 4-MBA-modified gold chip, where the sharp strong bands observed at about 1550 cm^{-1} and 1590 cm^{-1} are ascribed to the C=C aromatic stretching of the benzene ring. The strong peak at 1678 cm^{-1} is attributed to the carbonyl (C=O) stretching, and the peak at 1430 cm^{-1} due to the deformations of the C–O–H [34] indicates the presence of carboxylic groups on the SPR gold chip [35]. The above characterization results of EIS and FTIR-ATR data confirmed the modification of the gold chip with 4-MBA. This 4-MBA-modified SPR gold chip was utilized further for immobilization and sensing studies of Ebola virus.

Immobilization of EBOV-rNP on 4-MBA-modified gold SPR sensor chip for the screening of different mAbs of Ebola

Various steps were involved in the immobilization of EBOV-rNP on the 4-MBA-modified SPR gold chip, and this process comprised nine steps. In the first step, stabilization of baseline was performed for 120 s. For chemical binding between the 4-MBA adsorbed on the gold surface and free amino groups of EBOV-rNP, in the second step, activation of carboxyl groups of the 4-MBA-modified chip was carried out for 900 s with EDC/NHS. In the third step, washing was conducted with PBS, and the SPR angle shifted nearly to baseline [36]. In the fourth step, 0.04 mg mL^{-1} of EBOV-rNP was injected on the 4-MBA-modified gold chip, interacting for 1800 s,

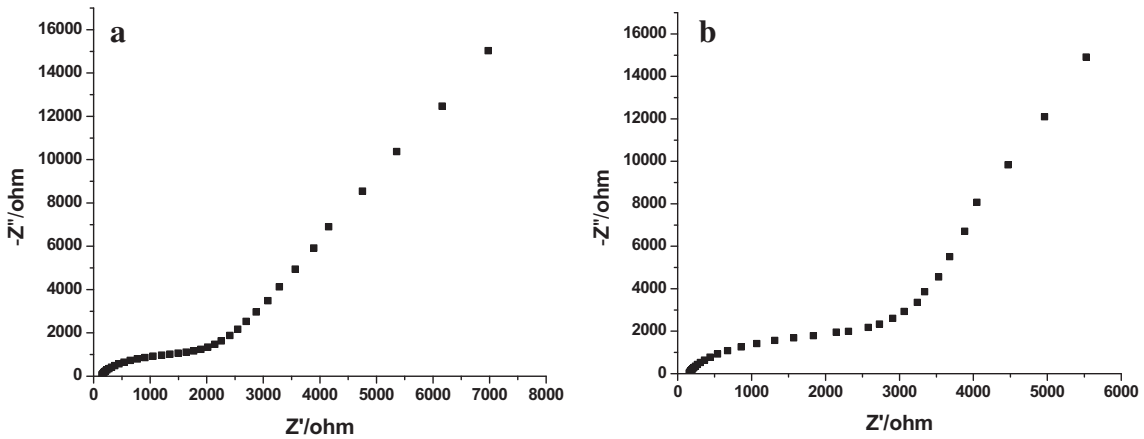

Fig. 2 (**a**) EIS spectra of the bare gold SPR chip and (**b**) the 4-MBA-modified gold SPR chip

Table 2 EIS parameters for the bare SPR gold chip and the 4-MBA-modified SPR gold chip

Electrodes	Solution resistance (ohm)	Charge transfer resistance (kΩ)	Capacitance (nF)
Bare gold chip	146.4	0.776	296.1
4-MBA-modified gold chip	160.0	1.078	0.830

and an increase in the SPR angle was observed. In the fifth step, washing was performed, and in the sixth step, to prevent nonspecific binding and also for the blocking of unreacted NHS ester groups on the 4-MBA chip, 1 M ethanolamine was used and allowed to react with the sensor surface for 600 s. In the seventh step, washing was performed for 30 s. In the eighth step, regeneration was carried out for 120 s. In the last (ninth) step, the back-to-baseline process was conducted for 60 s.

Interaction study of mAbs of Ebola with immobilized EBOV-rNP for screening of the best mAb

The EBOV-rNP-immobilized 4-MBA-modified sensor chip was utilized for the interaction of different concentrations (1:12,800, 1:6400, 1:3200, 1:1600 and 1:800) of mAb1, mAb2 and mAb3, and the results are depicted as an SPR sensorgram in Fig. 4A, B and C, respectively, showing the concentration-dependent angle changes at the various concentrations. The affinity interactions between immobilized EBOV-rNP and different mAbs was characterized by the affinity constant (K_D) expressed as an equilibrium dissociation constant. The data were fitted to a simple 1:1 L model [37, 38], A + B ↔ AB, where *A* is the analyte, *B* is the immobilized ligand and *AB* is the analyte–ligand complex. In the SPR system, the response signal (*R*) is proportional to the amount of analyte–ligand complex, and the R_{max} is proportional to the initial concentration of immobilized ligand on the 4-MBA-modified SPR chip.

The kinetic parameter K_D values were calculated for the binding of mAb1, mAb2 and mAb3 with immobilized EBOV-rNP using the kinetic analysis software, which revealed values of 809 nM, 350 pM and 52 pM, respectively; these low K_D values (if $K_D \leq 10$ nM) indicate high-affinity interactions of the mAb2 and mAb3 with the immobilized EBOV-rNP [39, 40]. The reactivity of all three mAbs against EBOV-rNP was also studied by indirect ELISA, which showed the best reactivity for mAb3 in terms of optical density (OD) (shown in Table 3). The ELISA results are in good agreement with the SPR K_D value. In view of the above, mAb3 is found to be the best high-affinity antibody, and hence is further utilized for developing the SPR sensing methodology for EBOV-rNP.

Immobilization of mAb3 on 4-MBA-modified gold SPR sensor chip

Figure 5A shows a graphical representation of the various steps involved in the immobilization of mAb3 on the 4-MBA-modified SPR gold chip; these nine steps are discussed

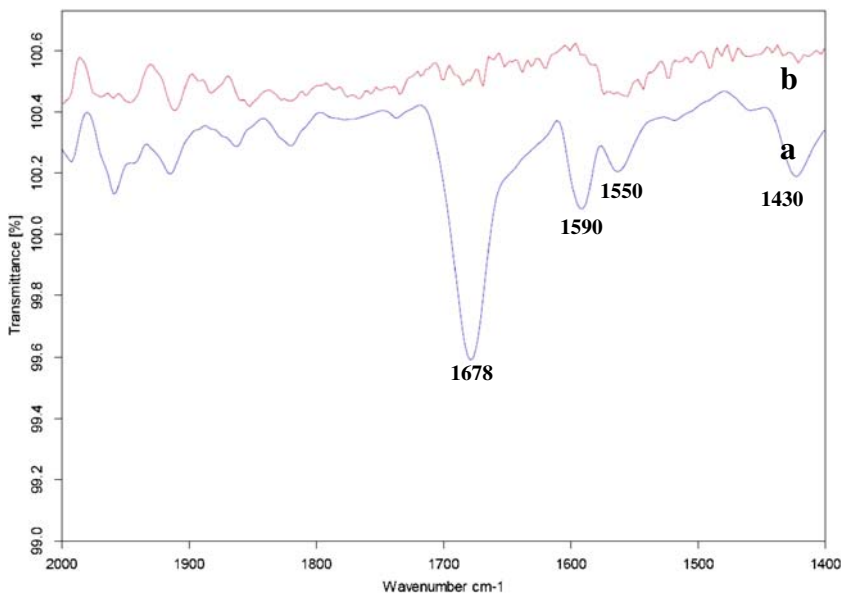

Fig. 3 FTIR-ATR spectra of the (**a**) bare gold SPR chip and (**b**) 4-MBA-modified gold SPR chip

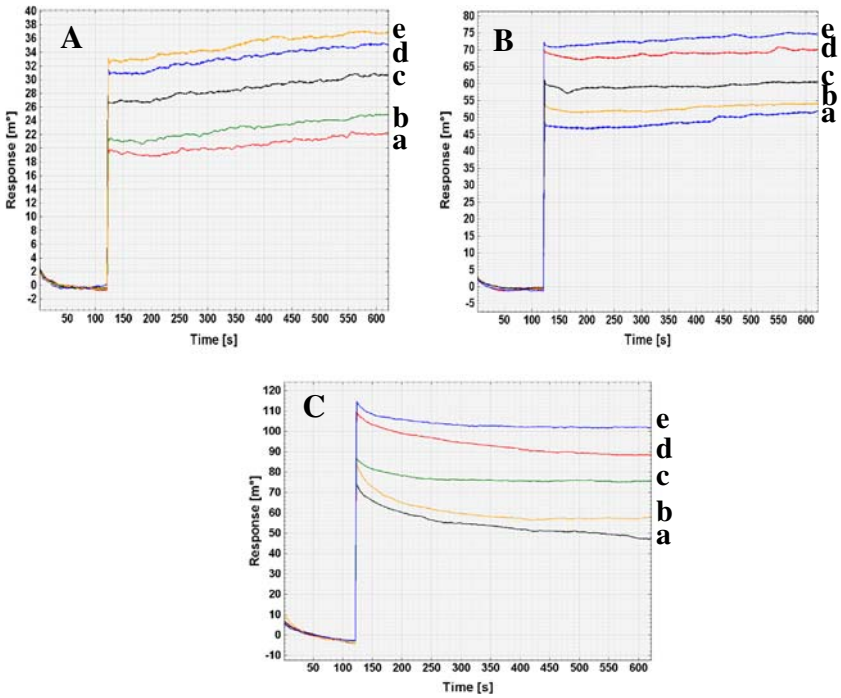

Fig. 4 SPR sensor response for the interaction of different dilutions of (**A**) mAb1, (**B**) mAb2 and (**c**) mAb3 with immobilized EBOV-rNP: dilutions of all mAbs are (**a**) 1:12,800, (**b**) 1:6400, (**c**) 1:3200, (**d**) 1:1600 and (**e**) 1:800

in detail in materials and methods of this paper. A net angle change of 213.27 m° is observed, which indicates the attachment of 1.77 ng/mm^2 of mAb3 on the 4-MBA SPR chip [41]. This mAb3-immobilized SPR chip was utilized to investigate the interaction of EBOV-rNP.

SPR characterization of immobilized mAb3 on 4-MBA-modified gold SPR sensor chip

The SPR angle before and after the anchoring of mAb3 on the 4-MBA-modified chip is illustrated in Fig. 5B, which shows that the SPR angle is shifted from 197.73 m° (Fig. 5a shows change in SPR angle after immobilization of 4-MBA) to 411 m° (Fig. 5b shows change in SPR angle after immobilization of mAb3 on the 4-MBA-modified SPR gold chip) due to the covalent attachment of mAb3 on the 4-MBA-modified gold chip [42, 43]. Thus, the change in SPR angle confirms the attachment of mAb3 on the 4-MBA-modified SPR gold chip.

Table 3 OD value of reactivity of all three mAbs against EBOV-rNP in the indirect ELISA format

Dilutions	mAb1	mAb2	mAb3
1:100	1.32	1.54	1.84
1:200	1.11	1.26	1.32
1:400	0.79	0.93	1.23
1:800	0.61	0.72	0.81
1:1600	0.41	0.43	0.54
PBS	0.07	0.09	0.05

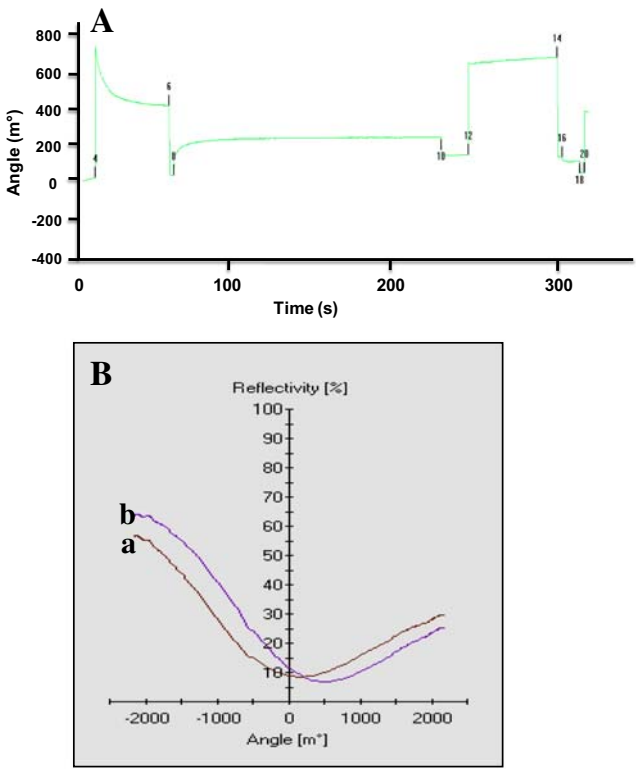

Fig. 5 (**A**) Sensorgram showing the steps involved in the immobilization of mAb3 of Ebola on a 4-MBA-modified SPR gold chip: (1) baseline, (2) EDC/NHS activation, (3) washing, (4) mAb3 coupling, (5) washing, (6) deactivation, (7) washing, (8) regeneration and (9) back to baseline; (**B**) SPR characterization of (a) 4-MBA/Au and (b) EBOV-rNP/4-MBA/Au

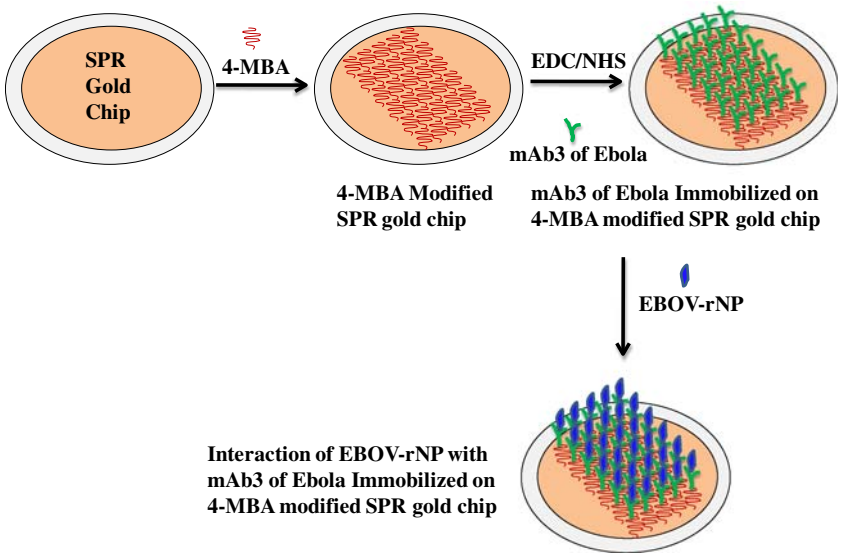

Fig. 6 Pictorial representation of steps involved in the development of the SPR sensing methodology for the EBOV-rNP

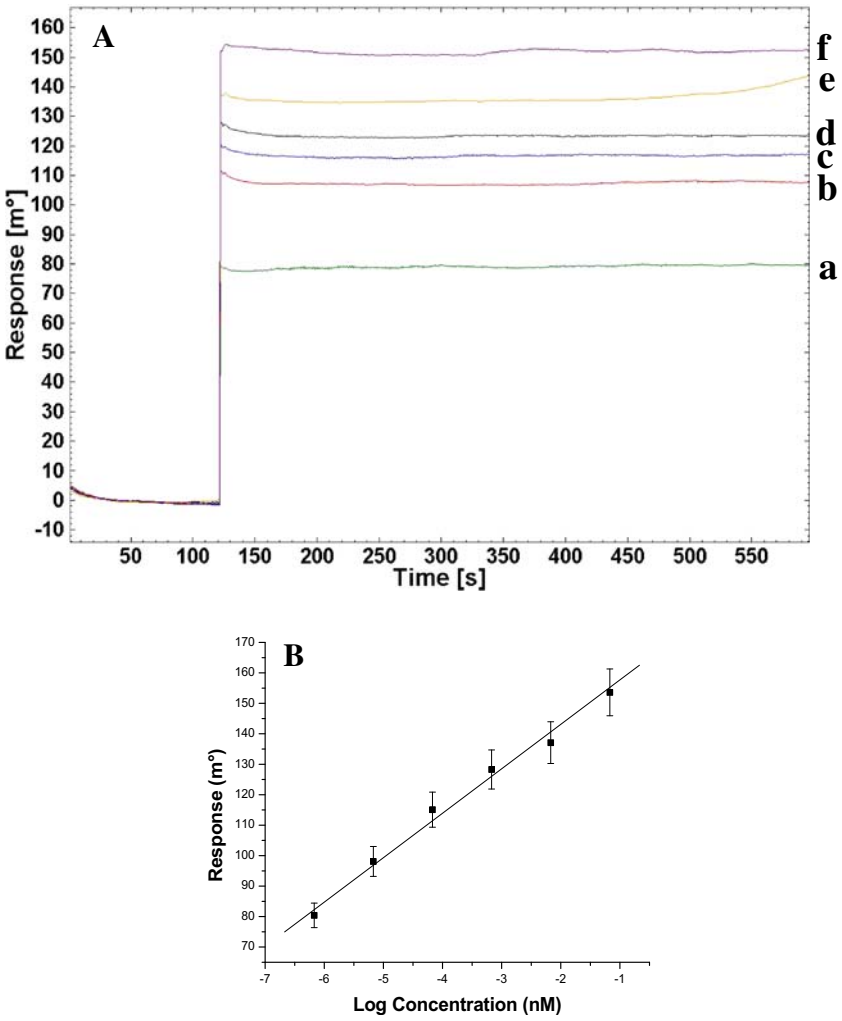

Fig. 7 SPR sensor response for the interaction of different dilutions of (**A**) EBOV-rNP: (**a**) 1:12,800, (**b**) 1:6400, (**c**) 1:3200, (**d**) 1:1600, (**e**) 1:800 and (**f**) 1:400 with immobilized mAb3 of Ebola, and (**B**) calibration graph for the response of angle changes against the log concentration of EBOV-rNP with immobilized mAb3. Temperature 25 °C and pH 7.5

Interaction study of EBOV-rNP with the immobilized mAb3

A schematic representation of the steps involved in the development of the SPR sensing methodology for the EBOV-rNP is shown in Fig. 6. The interaction study of mAb3 and EBOV-rNP was carried out at an optimized temperature of 25 °C and pH 7.5 (refer to sections S4 and S5 in the ESM for the details of optimized conditions). The mAb3-immobilized 4-MBA-modified sensor chip was utilized for the sensing of different concentrations of EBOV-rNP: 1:12800, 1:6400, 1:3200, 1:1600, 1:800 and 1:400, and the results are depicted as SPR sensorgrams in Fig. 7A. By analyzing the SPR curves, it was observed that the angle of the SPR increased with the increased concentration of EBOV-rNP. This increase in SPR response reflects the change in the dielectric constant of the environment between the mAb3 and EBOV-rNP. The limit of detection (LOD) with the present method was found to be 0.5 pg ml^{-1} for EBOV-rNP. A calibration curve was plotted using the SPR response in m° as a function of the logarithm of the EBOV-rNP concentrations shown in Fig. 7B. It shows a linear behavior when varying concentrations from 6.6×10^{-5} nM to 6.6 nM, with a coefficient of variation (R) of 99.51% and standard deviation (SD) of 0.5282% [37].

Analysis of equilibrium constants of Ebola virus mAb3 binding to EBOV-rNP

The affinity interactions between immobilized mAb3 and EBOV-rNP were characterized by the equilibrium constant (K_D). The data were fitted to a simple 1:1 L model [36, 44], A + B ↔ AB, where *A* is the analyte, *B* is the immobilized ligand and *AB* is the analyte–ligand complex. In the SPR system, the response signal (*R*) was proportional to the amount of analyte–ligand complex, and the R_{max} was proportional to the initial concentration of immobilized ligand on the 4-MBA-modified SPR chip. Hence, in this study, analysis of equilibrium constants K_D and *R*max was conducted for the binding of EBOV-rNP with immobilized mAb3 using kinetic analysis software, which showed values of 12.7 pM and 142.04 m°, respectively. This low K_D value (if $K_D \leq 10$ nM) indicates the high-affinity interactions of the EBOV-rNP with the immobilized mAb3 [39, 40]. It is worth noting here that the K_D value for the interaction of mAb3 with immobilized EBOV-rNP (refer to materials and methods section) was found to be 52 pM, which is higher than the K_D value of 12.7 pM for the reverse interaction (interaction of EBOV-rNP with immobilized mAb3). This indicates that the interaction of EBOV-rNP with immobilized mAb3 is much more effective than the interaction of mAb3 with immobilized EBOV-rNP, as reported earlier [45].

Thermodynamic analysis of EBOV-rNP binding to Ebola virus mAb3

The SPR experiment was conducted at different temperatures between 13 °C and 34 °C in increments of 3 °C in order to calculate K_D at the respective temperatures using kinetic evaluation software. Thermodynamic parameters ΔG, ΔH and ΔS were derived by substituting these K_D values in van 't Hoff Eqs. [46, 47].

$$\Delta G = -RT \ln K_A = \Delta H - T\Delta S \quad (1)$$

$$\Delta H = R\, T_2 T_1 / (T_2 - T_1) \ln K_2 / K_1 \quad (2)$$

$$K_A = 1/K_D \quad (3)$$

where *R* (universal gas constant), K_A (affinity constant expressed as equilibrium association constant), *T* (temperature), and K_1 and K_2 are affinity constants for temperature T_1 and T_2, respectively. ΔG, ΔH and ΔS are respectively the change in Gibb's free energy, change in enthalpy and change in entropy due to the binding of EBOV-rNP with the immobilized mAb3.

The ΔG for binding of EBOV-rNP to mAb3 was −17.54 kcal mol^{-1} at 298 K. The negative ΔG indicates spontaneous interaction of EBOV rNP with mAb3. Here, ΔH derived from the van 't Hoff Wizard in kinetic evaluation software was 155.0 kcal mol^{-1} for EBOV-rNP, and this reveals that the interaction of EBOV-rNP with mAb3 is an endothermic process [49]. ΔS for binding of EBOV-rNP with mAb3 was 579.47 cal mol^{-1} K^{-1}. The magnitude of TΔS values was found to be greater than the observed ΔH value, indicating that the net influence of enthalpy on EBOV-rNP with mAb3 is small, and that the apparent gain in entropy is actually the driver of the interaction of EBOV-rNP with mAb3 [48, 49]. The positive entropy in this study indicates a Langmuir-type isotherm [47, 50]. The Langmuir replacement reaction illustrates that the observed positive entropy is due to the removal of water molecules from either mAb3 or EBOV-rNP, or both, as reported elsewhere [51, 52]. The results for the above-described thermodynamic parameters reveal a lack of strong ionic interaction and confirm the high-affinity interactions of the EBOV-rNP with the immobilized mAb3, as reported elsewhere [53–55].

Conclusion

In summary, a real-time and label-free SPR technique was utilized for screening of different monoclonal antibodies (mAb1, mAb2 and mAb3) of Ebola virus for their affinity towards EBOV-rNP, and the best mAb was utilized for detection of EBOV-rNP using a 4-MBA-modified gold

SPR chip. FTIR-ATR spectra showed a modification of the SPR chip with 4-MBA. Affinity constant (K_D) values of 809 nM, 350 pM and 52 pM were found for the interaction of mAb1, mAb2 and mAb3 of Ebola with EBOV-rNP, respectively, which showed that mAb3 is the best antibody, and this was further confirmed by the ELISA results. The K_D for the interaction of mAb3 with EBOV-rNP was 52 pM, which is higher than the K_D value of 12.7 pM for the reverse interaction (interaction of EBOV-rNP with mAb3). This SPR result indicates that the interaction of EBOV-rNP with mAb3 is much more effective than the interaction of mAb3 with EBOV-rNP. The thermodynamic parameters ΔG, ΔH and ΔS were also determined for the interaction between mAb3 of Ebola and EBOV-rNP, and the values revealed that the interaction is a spontaneous, endothermic process driven by entropy. The LOD of the developed SPR methodology was found to be 0.5 pg ml^{-1} of EBOV-rNP with mAb3. In the future, the screened mAb3 will be used in our laboratory for the detection of Ebola virus in the serum of infected patients. This methodology may also yield valuable information for investigators developing biosensors and can also provide a framework for the evaluation of other BWA antibodies.

Acknowledgements The authors thank Dr. D. K. Dubey, Director, Defence Research and Development Establishment, DRDO, Gwalior-474002 (India), for his keen interest and encouragement. This manuscript is assigned DRDE accession no. DRDE/PD/31/2019.

Authors' contributions Pushpendra K. Sharma: conceptualization, methodology, validation, data analysis, investigation and manuscript writing. Jyoti S. Kumar: conceptualization, methodology, validation, formal analysis, investigation and manuscript writing (generation, purification and characterization of antigen and antibody used in this manuscript). Virendra V. Singh: review and editing. Utpal Biswas: methodology, validation and data analysis. Mannan Boopathi: conceptualization, methodology, writing (review and editing) and supervision. Paban K. Dash: conceptualization, methodology, editing and supervision. Kumaran Ganesan: review, editing and supervision. Rajiv Jain: review, editing and supervision. Shyam S. Sarkar and Syed I. Alam were involved in the characterization via FTIR-ATR and MALDI-TOF-TOF, respectively.

Funding By parent institution (DRDO, India).

Availability of data and material All data generated and materials used are provided in the manuscript.

Compliance with ethical standards

Ethics approval For animal experiments, the study protocol for all experiments was approved as protocol no. Viro-14/57/PKD by the Institutional Animal Ethics Committee (IAEC) constituted by the Committee for the Purpose of Control and Supervision of Experiments on Animals (CPCSEA), Ministry of Environment and Forestry, Government of India (regd. no. 37/GO/Rbi/S/99/CPCSEA).

Conflict of interest All authors state that there is no conflict of interest.

Consent for publication All authors give consent to publish this work.

References

1. Jansen HJ, Breeveld FJ, Stijnis C, Grobusch MP. Biological warfare, bioterrorism, and biocrime. Clin Microbiol Infect. 2014;20:488–96. https://doi.org/10.1111/1469-0691.12699.
2. Gire SK, Goba A, Andersen KG. Genomic surveillance elucidates Ebola virus origin and transmission during the 2014 outbreak. Science. 2014;345:1369–72. https://doi.org/10.1126/science.1259657.
3. World Health Organization. Investing to overcome the global impact of neglected tropical diseases: third WHO report on neglected tropical diseases 2015 (Vol. 3). World Health Organization. DOI: https://doi.org/10.1596/978-1-4648-0524-0/ch17.
4. World Health Organization. Ebola situation reports: Democratic Republic of the Congo. (2018) doi: https://doi.org/10.2807/1560-7917.
5. Gera P, Gupta A, Verma P, Singh J, Gupta J. Recent advances in vaccine development against Ebola threat as bioweapon. Virus Dis\. 2017;28:242–6. https://doi.org/10.1007/s13337-017-0398-0.
6. Baden LR, Kanapathipillai R, Campion EW, Morrissey S, Rubin EJ, Drazen JM. Ebola—an ongoing crisis. N Engl J Med. 2014;371:1458–9. https://doi.org/10.1056/NEJMe1411378.
7. Beeching NJ, Fenech M, Houlihan CF. Ebola virus disease. BMJ. 2014;349. https://doi.org/10.1136/bmj.g7348.
8. Nguyen VK, Binder SC, Boianelli A, Meyer-Hermann M, Hernandez-Vargas EA. Ebola virus infection modeling and identifiability problems. Front Microbiol. 2015;6:257–67. https://doi.org/10.3389/fmicb.2015.00257.
9. Duan D, Fan K, Zhang D, Tan S. Nanozyme-strip for rapid local diagnosis of Ebola. Biosens Bioelectron. 2015;74:134–41. https://doi.org/10.1016/j.bios.2015.05.025.
10. Kaushik A, Tiwari S, Jayant RD, Marty A, Nair M. Towards detection and diagnosis of Ebola virus disease at point-of-care. Biosens Bioelectron. 2016;75:254–72. https://doi.org/10.1016/j.bios.2015.08.040.
11. Butler D. Ebola experts seek to expand testing. Nat News. 2014;516:154. https://doi.org/10.1038/516154a.
12. Daaboul GG, Lopez CA, Chinnala J, Goldberg BB, Connor JH, Unlu MS. Digital sensing and sizing of vesicular stomatitis virus pseudotypes in complex media: a model for Ebola and Marburg detection. ACS Nano. 2014;8:6047–55. https://doi.org/10.1021/nn501312q.
13. Changula K, Yoshida R, Noyori O. Mapping of conserved and species-specific antibody epitopes on the Ebola virus nucleoprotein. Virus Res. 2013;176:83–90. https://doi.org/10.1016/j.virusres.2013.05.004.
14. Qiu X, Audet J, Wong G. Sustained protection against Ebola virus infection following treatment of infected nonhuman primates with ZMAb. Sci Rep. 2013;3:3365. https://doi.org/10.1038/srep03365.
15. Hussein HA, Hassan RY, El Nashar RM, Khalil SA, Salem SA, El-Sherbiny IM. Designing and fabrication of new VIP biosensor for the rapid and selective detection of foot-and-mouth disease virus (FMDV). Biosens Bioelectron. 2019;141:111467. https://doi.org/10.1016/j.bios.2019.111467.
16. Ro YT, Ticer A, Carrion R Jr, Patterson JL. Rapid detection and quantification of Ebola Zaire virus by one-step real-time quantitative reverse transcription-polymerase chain reaction. Microbiol Immunol. 2017;61:130–7. https://doi.org/10.1111/1348-0421.12475.

17. Cross RW, Ksiazek TG. ELISA methods for the detection of Ebola virus infection. In Ebola viruses, Humana Press, New York, NY. 2017:363–72. https://doi.org/10.1007/978-1-4939-7116-9_29.
18. Du K, Cai H, Park M. Multiplexed efficient on-chip sample preparation and sensitive amplification-free detection of Ebola virus. Biosens Bioelectron. 2017;91:489–96. https://doi.org/10.1016/j.bios.2016.12.071.
19. Giuffrida MC, Spoto G. Integration of isothermal amplification methods in microfluidic devices: recent advances. Biosens Bioelectron. 2017;90:174–86. https://doi.org/10.1016/j.bios.2016.11.045.
20. Zarei M. Infectious pathogens meet point-of-care diagnostics. Biosens Bioelectron. 2018;106:193–203. https://doi.org/10.1016/j.bios.2018.02.007.
21. Liu Xue CS, Erika G, Jiri H. Surface plasmon resonance biosensor for the ultrasensitive detection of bisphenol a. Anal Bioanal Chem. 2019;411:5655–8. https://doi.org/10.1007/s00216-019-01996-8.
22. Sina AAI, Vaidyanathan R, Wuethrich A, Carrascosa LG, Trau M. Label-free detection of exosomes using a surface plasmon resonance biosensor. Anal Bioanal Chem. 2019;411:1311–8. https://doi.org/10.1007/s00216-019-01608-5.
23. Zhou J, Qi Q, Wang C, Qian Y, Liu G, Wang Y, et al. Surface plasmon resonance (SPR) biosensors for food allergen detection in food matrices. Biosens Bioelectron. 2019;142:111449–64. https://doi.org/10.1016/j.bios.2019.111449.
24. Gupta G, Sharma PK, Sikarwar B, Merwyn S, Kaushik S, Boopathi M, et al. Surface plasmon resonance immunosensor for the detection of *Salmonella typhi* antibodies in buffer and patient serum. Biosens Bioelectron. 2012;36:95–102. https://doi.org/10.1016/j.bios.2012.03.046.
25. Gupta G, Bhaskar ASB, Tripathi BK, Pandey P, Boopathi M, Rao PVL, et al. Supersensitive detection of T-2 toxin by the in situ synthesized π-conjugated molecularly imprinted nanopatterns. An in situ investigation by surface plasmon resonance combined with electrochemistry. Biosens Bioelectron. 2011;26:2534–40. https://doi.org/10.1016/j.bios.2010.10.050.
26. Gupta G, Kumar A, Boopathi M. Rapid and quantitative determination of biological warfare agent *Brucella abortus* CSP-31 using surface plasmon resonance. Anal Bioanal Electrochem. 2011;3:26–37. https://doi.org/10.3390/s130708551.
27. Laemmli UK. Cleavage of structural proteins during the assembly of the head of bacteriophage T4. Nature. 1970;227:680. https://doi.org/10.1038/227680a0.
28. Brown RE, Jarvis KL, Hyland KJ. Protein measurement using bicinchoninic acid: elimination of interfering substances. Anal Biochem. 1989;180:136–9. https://doi.org/10.1016/0003-2697(89)90101-2.
29. Towbin H, Staehelin T. Gordon J electrophoretic transfer of proteins from polyacrylamide gels to nitrocellulose sheets: procedure and some applications. *Proc Natl Acad Sci*. 1979;76:4350–4. https://doi.org/10.1073/pnas.76.9.4350.
30. Köhler G, Milstein C. Continuous cultures of fused cells secreting antibody of predefined specificity. Nature. 1975;256:495. https://doi.org/10.1038/256495a0.
31. Lago S, Nadai M, Rossetto M, Richter SN. Surface plasmon resonance kinetic analysis of the interaction between G-quadruplex nucleic acids and an anti-G-quadruplex monoclonal antibody. Biochim. Biophys. Acta (BBA)-General Subjects. 2018;1862:1276–82. https://doi.org/10.1016/j.bbagen.2018.03.002.
32. Bard AJ, Faulkner LR, Leddy J, Zoski CG. Electrochemical methods: fundamentals and applications (Vol. 2). New York: Wiley; 1980.
33. Huang Y, Bell MC, Suni II. Impedance biosensor for peanut protein Ara h 1. Anal Chem. 2008;80:9157–61. https://doi.org/10.1021/ac801048g.
34. Ma C, Harris JM. Surface-enhanced Raman spectroscopy investigation of the potential-dependent acid−base chemistry of silver-immobilized 2-mercaptobenzoic acid. Langmuir. 2011;27:3527–33. https://doi.org/10.1021/la1044859.
35. Rosendahl SM, Burgess IJ. Electrochemical and infrared spectroscopy studies of 4-mercaptobenzoic acid SAMs on gold surfaces. Electrochim Acta. 2008;53:6759–67. https://doi.org/10.1016/j.bios.2016.03.038.
36. Mohseni S, Moghadam TT, Dabirmanesh B, Jabbari S, Khajeh K. Development of a label-free SPR sensor for detection of matrixmetalloproteinase-9 by antibody immobilization on carboxymethyldextran chip. Biosens Bioelectron. 2016;81:510–6. https://doi.org/10.1016/j.bios.2016.03.038.
37. Chiu NF, Fan SY, Yang CD, Huang TY. Carboxyl-functionalized graphene oxide composites as SPR biosensors with enhanced sensitivity for immunoaffinity detection. Biosens Bioelectron. 2017;89:370–6. https://doi.org/10.1016/j.bios.2016.06.073.
38. Babu HKRR, Gheber LA. Fluorescence-based kinetic analysis of miniaturized protein microarrays. Biosens Bioelectron. 2018;122:290–9. https://doi.org/10.1016/j.bios.2018.09.05.
39. Retra K, Irth H, van Muijlwijk-Koezen JE. Surface plasmon resonance biosensor analysis as a useful tool in FBDD. Drug Discov Today Technol. 2010;7:e181–7. https://doi.org/10.1016/j.ddtec.2010.11.01.
40. Wassaf D, Kuang G. High-throughput affinity ranking of antibodies using surface plasmon resonance microarrays. Anal Biochem. 2006;351:241–53. https://doi.org/10.1016/j.ab.2006.01.043.
41. Primo EN, Bollo S, Rubianes MD, Rivas GA. Immobilization of graphene-derived materials at gold surfaces: towards a rational design of protein-based platforms for electrochemical and plasmonic applications. Electrochim Acta. 2018;259:723–32. https://doi.org/10.1016/j.electacta.2017.10.184.
42. Sadana A, Sadana N. Handbook of biosensors and biosensor kinetics. Elsevier. 2010. https://doi.org/10.1080/00107514.2011.603431.
43. Touhami A. Biosensors and nanobiosensors: design and applications. Nanomedicine. 2014;15:374–403. https://doi.org/10.1039/b718174d.65.
44. Liu JT, Chen LY, Shih MC, Chang Y, Chen WY. The investigation of recognition interaction between phenylboronate monolayer and glycated hemoglobin using surface plasmon resonance. Anal Biochem. 2008;375:90–6. https://doi.org/10.1016/j.ab.2008.01.004.
45. Sikarwar B, Sharma PK, Saraswat S, Athmaram TN, Boopathi M, Singh B, et al. Surface plasmon resonance immunosensor for recombinant H1N1 protein. Plasmonics. 2015;10:77–85. https://doi.org/10.1007/s11468-014-9780-6.
46. Kuroki K, Maenaka K. Analysis of receptor–ligand interactions by surface plasmon resonance. Totowa, NJ: In Immune Receptors Humana Press; 2011. p. 83–106. https://doi.org/10.1007/978-1-61779-139-06.
47. Myszka DG. Kinetic, equilibrium, and thermodynamic analysis of macromolecular interactions with BIACORE. Methods Enzymol Academic Press. 2000;323:325–40. https://doi.org/10.1016/S0076-6879(00)23372-7.
48. Wang W, Zhu Y, Chen T, Zhou G. Kinetic and thermodynamic analysis of ultra-high pressure and heat-induced denaturation of bovine serum albumin by surface plasmon resonance. Trop J Pharm Res. 2017;16:1965–72. https://doi.org/10.4314/tjpr.v16i8.29.
49. Khalili H, Brocchini S, Khaw PT, Filippov SK. Comparative thermodynamic analysis in solution of a next generation antibody mimetic to VEGF. RSC Adv. 2018;8:35787–93. https://doi.org/10.1039/C8RA07059H.
50. Bostrom J, Haber L, Koenig P, Kelley RF, Fuh G. High affinity antigen recognition of the dual specific variants of herceptin is

entropy-driven in spite of structural plasticity. PLoS One. 2011;6: e17887. https://doi.org/10.1371/journal.pone.0017887.

51. Hearty S, Leonard P, O'Kennedy R. Measuring antibody–antigen binding kinetics using surface plasmon resonance. Totowa, N.J.: In Antibody Engineering Humana Press; 2012. p. 411–42. https://doi.org/10.1007/978-1-61779-974-7_24.
52. Altschuh D, Dubs MC, Weiss E, Zeder-Lutz G, Van Regenmortel MH. Determination of kinetic constants for the interaction between a monoclonal antibody and peptides using surface plasmon resonance. Biochemistry. 1992;31:6298–304. https://doi.org/10.1021/bi00142a019.
53. Rempel B, Gui B, Maley J, Reaney M, Sammynaiken R, Biomolecular Interaction Study of Cyclolinopeptide A with Human Serum Albumin. BioMed Research International. 2010; 2010: Article ID 737289J. https://doi.org/10.1155/2010/737289.
54. Van Oss CJ, Hydrophobic, hydrophilic and other interactions in epitope-paratope binding. Molecular Immunology.1995;32:199–211. https://doi.org/10.1016/0161-5890(94)00124-J.
55. Pérez-Gramatges, A, Argüelles-Monal, W, Peniche-Covas, C Thermodynamics of complex formation of polyacrylic acid with poly(N-vinyl-2-pyrrolidone) and chitosan . Polymer Bulletin. 1996; 37: 127–134. https://doi.org/10.1007/BF00313828.